Stress hybrid finite elements with multiple embedded cracks

O.L. Manzoli
Department of Civil Engineering, State University of São Paulo, Bauru-SP, Brazil.

P.B. Shing
Department of Civil Engineering, University of Colorado, Boulder-CO, U.S.A.

ABSTRACT: A technique to embed multiple displacement discontinuities and non-uniform discontinuity modes into stress hybrid elements is presented. This technique is an effort to make the stress hybrid elements suitable for fracture mechanics analyses, extending the capabilities of the embedded discontinuity finite elements.

Keywords: stress hybrid finite element, embedded cracks, non-uniform modes, multiple cracks.

1 INTRODUCTION

During the last few years, embedded displacement discontinuity elements have been shown to be an effective tool to describe the propagation of cracks independent of element boundaries (Dvorkin et al. 1990, Klisinski et al. 1991, Lotfi & Shing 1995, Oliver 1996b, Alfaiate et al. 2002, Spencer & Shing 2002). Most of the work has been devoted to embed discontinuities into displacement-based finite elements (Jirásek 2000).

The stress hybrid finite element of Pian (1995) has been recognized by its better performance in relieving shear and incompressibility lockings. These benefits may be also desirable in fracture mechanics analyses. The first attempt to use this class of elements for embedded discontiunity has been made by Spencer and Shing (2002) by means of a variational principle that accounts for a crack line in the element interior.

In this paper an alternative technique to embed displacement discontinuities into these elements is presented. The technique follows the general procedure to embed discontinuities into finite elements as presented by Manzoli & Shing (2002). In contrast to the formulation of Spencer and Shing (2002), the approach used here retains the original variational principle used to derive the underlying element for the continuous portion of the element that is crossed by a crack line. The resulting formulation can be easily extended to account for multiple discontinuities in the element, as well as non-uniform discontinuity modes. As it is shown in this paper, the later capability can be essential to prevent stress locking when the element is subjected to bending-type deformation.

Numerical tests are presented to access the performance of the resulting formulation.

2 DECOMPOSITION OF THE DISPLACEMENT FIELD

The displacement field, $\mathbf{u}$, of a finite element divided by a discontinuity interface S (Fig. 1) can be decomposed into a component associated with the deformation of the continuous portion, $\mathbf{u}^C$, and a component related to the rigid-body relative motion, $\mathbf{u}^R$, between the two parts of the element:

$$\mathbf{u} = \mathbf{u}^C + \mathbf{u}^R \tag{1}$$

with

$$\mathbf{u}^R = \mathcal{H}(x)[[\mathbf{u}]] \tag{2}$$

where x is the coordinate of a material point in the element according to an interface coordinate system (x, y), such that the x axis is normal to the discontinuity interface (Fig. 1.a). $\mathcal{H}$ is the Heaviside function defined in the domain of the

element ($\mathcal{H}(x) = 1$ if $x > 0$ and $\mathcal{H}(x) = 0$ otherwise) and $[[\mathbf{u}]]$ is the vector containing the components of the displacement discontinuity at the interface, which has been assumed uniform in the element.

The values of the $\mathbf{u}^R$ evaluated at the nodes of the element can be grouped into a vector $\mathbf{d}^R$, such that

$$\mathbf{d}^R = \mathbf{P}[[\mathbf{u}]] \tag{3}$$

in which the P matrix collects the values of the Heaviside function at the element nodes:

$$\mathbf{P} = \begin{bmatrix} \mathcal{H}(x_1) & 0 \\ 0 & \mathcal{H}(x_1) \\ \vdots & \vdots \\ \mathcal{H}(x_{n_{ed}}) & \\ & \mathcal{H}(x_{n_{ed}}) \end{bmatrix} \tag{4}$$

where n_{ed} is the number of element nodes and x_i (i = 1,2, n_{ed}) are the nodal coordinates.

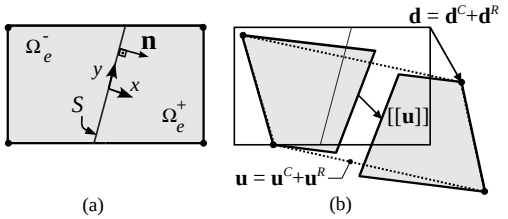

Figure 1. Decomposition of the displacement field .

3 STRESS HYBRID FINITE ELEMENT

Consider the equilibrium of a two-dimensional body Ω located in a coordinate system (X,Y). The body is supported on the boundary Γ_u with prescribed displacements, $\mathbf{u}^\Gamma$, and is subjected to prescribed traction, $\mathbf{t}^\Gamma$, on Γ_t ($\Gamma_u \cup \Gamma_t = \Gamma$, $\Gamma_u \cap \Gamma_t = \varnothing$). The body is also subjected to externally applied body forces **b**.

Let **u** be the displacement field of the body. The strain field corresponding to **u** is

$$\boldsymbol{\varepsilon} = \mathbf{D}\,\mathbf{u} \tag{5}$$

where **D** is the differential operator on **u** to obtain the strain components.

The continuum is assumed linearly elastic, so that the corresponding stress field is given by

$$\boldsymbol{\sigma} = \mathbf{E}\boldsymbol{\varepsilon} \tag{6}$$

where **E** is the elastic stress-strain material matrix.

3.1 *Hybrid variational functional*

The Hellinger-Reissner variational principle for the continuum can be expressed as

$$\Pi = \int_\Omega \left[-\frac{1}{2}\boldsymbol{\sigma}^{\mathrm{T}}\mathbf{E}^{-1}\boldsymbol{\sigma} - (\mathbf{D}^{\mathrm{T}}\,\boldsymbol{\sigma})^{\mathrm{T}}\,\mathbf{u} - \mathbf{b}^{\mathrm{T}}\,\mathbf{u} \right] d\Omega + \int_{\Gamma_t} (\mathbf{t} - \mathbf{t}^\Gamma)^{\mathrm{T}}\,\mathbf{u}\, d\Gamma - \int_{\Gamma_u} \mathbf{t}^{\mathrm{T}}\mathbf{u}^\Gamma\, d\Gamma = \text{stationary} \tag{7}$$

where **t** is the boundary traction vector that is obtained from $\boldsymbol{\sigma}$. Assuming that the boundary condition

$$\mathbf{u} = \mathbf{u}^\Gamma \text{ on } \Gamma_u \tag{8}$$

and the equilibrium equation

$$\mathbf{D}^{\mathrm{T}}\boldsymbol{\sigma} + \mathbf{b} = \mathbf{0} \tag{9}$$

are satisfied *a priori*, the variational functional (Eq. 7) becomes:

$$\Pi' = -\int_\Omega \frac{1}{2}\boldsymbol{\sigma}^{\mathrm{T}}\mathbf{E}^{-1}\boldsymbol{\sigma}\, d\Omega + \int_\Gamma \mathbf{t}^{\mathrm{T}}\mathbf{u}\, d\Gamma - \int_{\Gamma_t} \mathbf{t}^{\Gamma\,\mathrm{T}}\mathbf{u}\, d\Gamma = \text{stationary} \tag{10}$$

in which the stresses and the boundary displacements are the independent variables.

3.2 *Finite element approximation*

For sake of simplicity, consider a quadrilateral four-node finite element with boundaries aligned with the global coordinate axis (X, Y). The stresses in the element interior can be interpolated by five parameters, a_i (i=1,2,..,5), as follows:

$$\boldsymbol{\sigma} = \mathbf{S}\,\mathbf{a} \tag{11}$$

with

$$\boldsymbol{\sigma}^{\mathrm{T}} = [\sigma_{XX} \quad \sigma_{YY} \quad \sigma_{XY}] \tag{12}$$

$$\mathbf{a}^{\mathrm{T}} = [a_1 \quad a_2 \quad a_3 \quad a_4 \quad a_5] \tag{13}$$

$$\mathbf{S} = \begin{bmatrix} 1 & 0 & 0 & Y & 0 \\ 0 & 1 & 0 & 0 & X \\ 0 & 0 & 1 & 0 & 0 \end{bmatrix} \tag{14}$$

Note that the equilibrium condition (Eq. 9) is fulfilled for the adopted stress interpolation.

The element traction vector can be expressed in terms of the stress parameters as:

$$\mathbf{t} = \boldsymbol{\mathcal{N}}_{\nu}\boldsymbol{\sigma} = \boldsymbol{\mathcal{N}}_{\nu}\mathbf{S}\,\mathbf{a} = \mathbf{R}\,\mathbf{a} \tag{15}$$

in which

$$\boldsymbol{\mathcal{N}}_{\nu} = \begin{bmatrix} \nu_X & 0 & \nu_Y \\ 0 & \nu_Y & \nu_X \end{bmatrix} \tag{16}$$

where ν_X and ν_Y are the components of the unit vector, $\boldsymbol{\nu}$, normal to the element boundary.

The boundary displacement are approximated by linear interpolation of the nodal displacements, as follows

$$\mathbf{u} = \mathbf{L}\,\mathbf{d} \tag{17}$$

where $\mathbf{L}$ is the boundary displacement interpolation matrix and $\mathbf{d}$ is the vector collecting the nodal displacements.

Substituting Equations 11, 15 and 17 into the Equation 10, we obtain

$$\Pi' = -\frac{1}{2}\mathbf{a}^{\mathrm{T}}\mathbf{H}\,\mathbf{a} + \mathbf{a}^{\mathrm{T}}\mathbf{G}\,\mathbf{d} - \mathbf{f}_{ext}^{\mathrm{T}} \tag{18}$$

where

$$\mathbf{H} = \int_{\Omega_e} \mathbf{S}^{\mathrm{T}}\mathbf{E}^{-1}\mathbf{S}\,d\Omega \tag{19}$$

$$\mathbf{G} = \oint_{\Gamma_e} \mathbf{R}^{\mathrm{T}}\mathbf{L}\,d\Gamma \tag{20}$$

$$\mathbf{f}_{ext} = \int_{\Gamma_{et}} \mathbf{L}^{\mathrm{T}}\mathbf{t}^{\Gamma}\,d\Gamma \tag{21}$$

where Ω_e is the element domain, Γ_e is the element boundary and Γ_{et} is the element boundary with prescribed traction.

Stationarity of the potential functional (Eq. 18) with respect to the stress parameters $\mathbf{a}$ yields

$$-\mathbf{H}\mathbf{a} + \mathbf{G}\mathbf{d} = \mathbf{0} \tag{22}$$

from which it is possible to express the stress parameters in terms of the nodal displacements:

$$\mathbf{a} = \mathbf{H}^{-1}\mathbf{G}\,\mathbf{d} \tag{23}$$

Substituting Equation 23 into Equation 11, we obtain the stresses as

$$\boldsymbol{\sigma} = \mathbf{S}\,\mathbf{H}^{-1}\mathbf{G}\,\mathbf{d} \tag{24}$$

The corresponding strains are given by

$$\boldsymbol{\varepsilon} = \mathbf{E}^{-1}\,\boldsymbol{\sigma} = \mathbf{E}^{-1}\,\mathbf{S}\,\mathbf{H}^{-1}\,\mathbf{G}\,\mathbf{d} = \mathbf{B}^{H}\,\mathbf{d} \tag{25}$$

Taking the variation of the potential functional (Eq. 18) with respect to the nodal displacements $\mathbf{d}$, and considering Equation 23, we obtain the element internal force vector,

$$\mathbf{f}_{int} = \mathbf{K}^{H}\mathbf{d} \tag{26}$$

where $\mathbf{K}^{H} = \mathbf{G}^{\mathrm{T}}\,\mathbf{H}^{-1}\,\mathbf{G}$ is the stiffness matrix of the Pian element.

3.3 *Embedded displacement discontinuity element*

If the element is crossed by a discontinuity interface, we must ensure that a total relaxation of the continuous portion of the element takes place if the nodal displacements $\mathbf{d}$ is entirely due to the rigid-body motion caused by the displacement discontinuity, i.e.

$$\boldsymbol{\sigma} = 0 \;\text{ if }\; \mathbf{d} = \mathbf{d}^{R}\,(=\mathbf{P}\,[[\mathbf{u}]]) \tag{27}$$

Note that this condition is fulfilled provided that

$$\mathbf{a} = \mathbf{H}^{-1}\,\mathbf{G}\,(\mathbf{d} - \mathbf{P}\,[[\mathbf{u}]]) \tag{28}$$

in place of Equation 23. Equation 28 means that only the continuous part of the displacement field has been considered in the functional (18).

In this case, the stresses, strains and the internal forces are respectively given by

$$\boldsymbol{\sigma}^{C} = \mathbf{E}\,\mathbf{B}^{H}\,(\mathbf{d} - \mathbf{P}\,[[\mathbf{u}]]) \tag{29}$$

$$\boldsymbol{\varepsilon}^{C} = \mathbf{B}^{H}\,(\mathbf{d} - \mathbf{P}\,[[\mathbf{u}]]) \tag{30}$$

$$\mathbf{f}_{int} = \mathbf{K}^{H}\,(\mathbf{d} - \mathbf{P}\,[[\mathbf{u}]]) \tag{31}$$

4 NON-LINEAR BEHAVIOR OF THE DISCONTINUITY INTERFACE

4.1 *Non-linear fracture mechanics*

The non-linear behavior of the discontinuity interface can be described by means of a constitutive relation between the cohesive traction in the interface, $\mathbf{t}_S$, and the components of the displacement jump, $[[\mathbf{u}]]$. In non-linear fracture mechanics, this constitutive relation is given by an *adhoc* discrete law of the form:

$$\mathbf{t}_S = \Sigma^{d}\,([[\mathbf{u}]]) \tag{32}$$

where $\Sigma^{d}(\bullet)$ gives the traction as a function of the displacement jump and its history .

4.2 *Strong discontinuity approach*

In the so-called strong discontinuity approach (Simo et al. 1993, Oliver et al. 1999), the behavior

of the interface is described by a continuum (stress-strain) non-linear constitutive law. A discrete constitutive law is induced by degenerating the continuum in a consistent manner. In this case, the traction vector in the interface is given by:

$$\mathbf{t}_S = \boldsymbol{\mathcal{N}}_{\mathbf{n}}\, \Sigma^c(\boldsymbol{\varepsilon}_S) \quad \text{in} \quad S \tag{33}$$

where $\Sigma^c(\bullet)$ returns the stresses from the strains evaluated in S, $\boldsymbol{\varepsilon}_S$. The $\boldsymbol{\mathcal{N}}_{\mathbf{n}}$ matrix contains zeros and the components of the unit vector normal to the interface discontinuity, **n**, according to the structure of Equation 16.

The total strain field is obtained from the discontinuous displacement field, which can be recovered as follows:

$$\mathbf{u} = \mathbf{u}^C + \mathbf{u}^R = \mathbf{u}^C + \mathcal{H}(x)\,[[\mathbf{u}]] \tag{34}$$

Taking the gradient of Equation 34 leads to the corresponding strain field:

$$\boldsymbol{\varepsilon} = \boldsymbol{\varepsilon}^C + \delta_S\, \boldsymbol{\mathcal{N}}_{\mathbf{n}}^{\mathrm{T}}\, [[\mathbf{u}]] \tag{35}$$

where δ_S is the Dirac delta distribution placed in S.

The last term of Equation 35 introduces an unbounded component in the total strain field.

Thus, taking into account Equation 30 and Equation 35, the Equation 33 becomes:

$$\mathbf{t}_S = \boldsymbol{\mathcal{N}}_{\mathbf{n}} \Sigma^c \left(\mathbf{B}^H (\mathbf{d} - \mathbf{P}\,[[\mathbf{u}]]) + \frac{1}{k} \boldsymbol{\mathcal{N}}_{\mathbf{n}}^{\mathrm{T}}\, [[\mathbf{u}]] \right) \tag{36}$$

For computational purposes, in Equation 36, the value of δ_S in S has been replaced by the approximation (Oliver 1996):

$$\delta_S(\mathbf{x}) \approx \begin{cases} \dfrac{1}{k} & \text{if } \mathbf{x} \in S, \\ 0 & \text{otherwise.} \end{cases} \tag{37}$$

so that, when delta regularization parameter, k, tends to zero, the approximation in Equation 37 transforms into an exact Dirac delta distribution.

4.2.1 *Constitutive model for the interface*

In the strong discontinuity approach, the non-linear behavior in the interface can be described by a continuum-type constitutive law. In this paper, we use a standard associative elastoplastic constitutive model that can be described by the following set of incremental equations (Simo & Hughes 1998):

$$\dot{\boldsymbol{\sigma}} = \mathbf{E}\,(\dot{\boldsymbol{\varepsilon}} - \dot{\boldsymbol{\varepsilon}}^p) \tag{38}$$

$$\dot{\boldsymbol{\varepsilon}}^p = \dot{\lambda} \frac{\partial \phi}{\partial \boldsymbol{\sigma}} \tag{39}$$

$$\dot{q} = H(\lambda)\, \dot{\lambda} \tag{40}$$

where $\boldsymbol{\varepsilon}^p$ is the plastic strains, ϕ is the yield function, q is the stress like internal variable, H is the hardening/softening modulus and $\dot{\lambda}$ is the plastic multiplier.

The loading and unloading situations are distinguished by the Kuhn-Tucker conditions:

$$\phi(\boldsymbol{\sigma}, q) \le 0, \quad \dot{\lambda} \ge 0, \quad \dot{\lambda}\, \phi(\boldsymbol{\sigma}, q) = 0 \tag{41}$$

where ϕ defines the elastic domain $\phi(\boldsymbol{\sigma},q) \le 0$.

To make the constitutive law compatible with strong discontinuity, the plastic multiplier and the inverse of the H modulus must have a distributional character (Simo et al. 1993), i.e.:

$$\lambda = \delta_S\, \bar{\lambda} \approx \frac{1}{k} \bar{\lambda}; \tag{42}$$

$$\frac{1}{H(\lambda)} = \delta_S \frac{1}{\bar{H}(\bar{\lambda})} \approx \frac{1}{k} \frac{1}{\bar{H}(\bar{\lambda})} \tag{43}$$

The following expressions for the yield surface and softening law are adopted:

$$\phi(\boldsymbol{\sigma}, q) = \sqrt{\frac{2}{3}}\, \|\mathbf{S}\| + p - q \tag{44}$$

$$\bar{H}(\bar{\lambda}) = -0.95 \frac{f_t^{\,2}}{G_F} e^{-\frac{f_t}{G_F}\bar{\lambda}} \tag{45}$$

where **S** stands for the deviatoric stresses, p is the mean stress, f_t is the tensile strength and G_F is the fracture energy.

5 COUPLING CONTINUUM AND INTERFACE

The continuum and the interface can be coupled by means of the following condition:

$$\mathbf{t}_S - \boldsymbol{\mathcal{N}}_{\mathbf{n}}\, \boldsymbol{\sigma}^C = \mathbf{0} \quad \text{in } Q \in S \tag{46}$$

which enforces the traction continuity at a collocation point Q of the discontinuity interface (Figure 2.a).

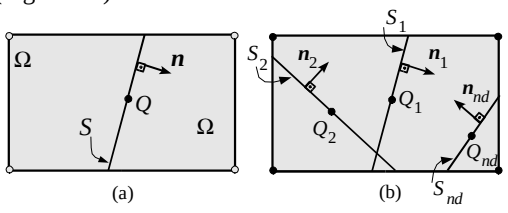

Figure 2. Collocation points: a) single interface b) multiple interfaces.

Taking into account the constitutive relation for the continuum (Eq. 29), the equilibrium equations, Equation 46, become:

$$\mathbf{t}_S(\mathbf{d},[[\mathbf{u}]]) - \mathbf{K}^S(\mathbf{d} - \mathbf{P}[[\mathbf{u}]]) = \mathbf{0} \quad \text{at } Q \in S \tag{47}$$

where

$$\mathbf{K}^S = \mathcal{N}_\mathbf{n}\,\mathbf{E}\,\mathbf{B}^H \tag{48}$$

and the expression of $\mathbf{t}_S(\mathbf{d},[[\mathbf{u}]])$ is given by Equation 32 for the discrete interface approach or by Equation 36 for the regularized strong discontinuity approach.

6 MULTIPLE DISCONTINUITIES

If more than one discontinuity interface is present in the element (Fig. 2.b), the resulting rigid-body motion is the sum of those related to each interface:

$$\mathbf{u}^R = \sum_{k=1}^{nd} \mathcal{H}_k [[\mathbf{u}]]_k \tag{49}$$

where *nd* is the number of discontinuity interfaces in the element. $\mathcal{H}_k$ and $[[\mathbf{u}]]_k$ are the Heaviside function and the discontinuity modes of the *k*th discontinuity interface, S_k.

The corresponding nodal displacement vector is given by:

$$\mathbf{d}^R = [\mathbf{P}]\{[[\mathbf{u}]]\} \tag{50}$$

where the multiple-discontinuity matrix [**P**] and the vector {[[**u**]]} collect, respectively, the **P** matrices and [[**u**]] vectors for the individual interfaces.

The traction continuity (Eq. 47) must be written for a collocation point in each interface of the element (Fig. 2.b), yielding the following set of equations:

$$\{\mathbf{t}_S(\mathbf{d},[[\mathbf{u}]])\} - [\mathbf{K}^S](\mathbf{d} - [\mathbf{P}]\{[[\mathbf{u}]]\}) = 0 \tag{51}$$

where

$$\{\mathbf{t}_S\}^{\mathrm{T}} = \{\ \mathbf{t}_{S_1} \quad \mathbf{t}_{S_2} \quad \dots \quad \mathbf{t}_{S_{nd}}\ \} \tag{52}$$

$$[\mathbf{K}^S]^{\mathrm{T}} = \left[\ \mathbf{K}_1^S \quad \mathbf{K}_2^S \quad \dots \quad \mathbf{K}_{nd}^S\ \right] \tag{53}$$

group, respectively, the traction vectors, $\mathbf{t}_{Sj}$, and the $\mathbf{K}^S_j$ matrices for each collocation point Q_j (j = 1, 2, ..., *nd*).

7 NON-UNIFORM DISCONTINUITY MODES

Consider an interface discontinuity with two collocation points, Q_1 and Q_2, as shown in Figure 3.

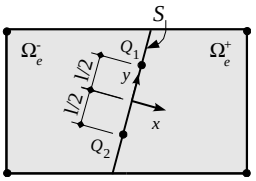

Figure 3. Collocation points: single interface with non-uniform discontinuity modes.

Each collocation point introduces a discontinuity jump, $[[\mathbf{u}]]_i$ (i = 1,2). It is possible to define $\mathbf{P}_1$ and $\mathbf{P}_2$ matrices related to the collocation points, such that:

$$\mathbf{d}^R = [\mathbf{P}]\{[[\mathbf{u}]]\} \tag{54}$$

where

$$[\mathbf{P}] = [\mathbf{P}_1 \quad \mathbf{P}_2] \tag{55}$$

$$\{[[\mathbf{u}]]\}^{\mathrm{T}} = \{[[\mathbf{u}]]_1 \ \ [[\mathbf{u}]]_2\} \tag{56}$$

Writing the traction continuity (Eq. 47) for each collocation point, the resulting formulation is identical to that described for the multiple-discontinuity approach.

The $\mathbf{P}_1$ and $\mathbf{P}_2$ matrices can be written as:

$$\mathbf{P}_j = \begin{bmatrix} M_j(\mathbf{x}_1) & 0 \\ 0 & M_j(\mathbf{x}_1) \\ \vdots & \vdots \\ M_j(\mathbf{x}_{n_{en}}) & 0 \\ 0 & M_j(\mathbf{x}_{n_{en}}) \end{bmatrix} \ (j = 1,2) \tag{57}$$

where $\mathbf{x}_i$ (i = 1,2,…,*nd*) are the nodal coordinates according to the interface system (x,y). For instance, the functions $M_j(\mathbf{x})$ can be constructed from the linear interpolation functions on S as shown in Figure 4:

$$M_1(\mathbf{x}) = \mathcal{H}(x)\frac{l/2 + y}{l};\ M_2(\mathbf{x}) = \mathcal{H}(x)\frac{l/2 - y}{l} \tag{58}$$

where l is the distance between the two collocation points.

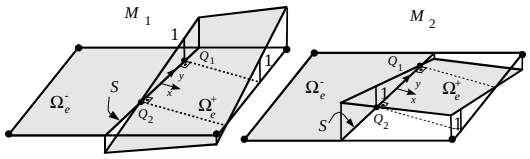

Figure 4. Linear interpolation functions M_1 and M_2.

8 SOLUTION SCHEME

For the embedded multiple discontinuities formulation, the equilibrium equations in the element level are given by Equations 31 and 51, relating the variables of an element at the *i*th iteration of the *n*th loading step:

$$\mathbf{f}_{int}^{n,i} = \mathbf{K}^{H}(\mathbf{d}^{n,i} - [\mathbf{P}]\{[[\mathbf{u}]]\}^{n,i}) \tag{59}$$

$$\begin{aligned}&\left\{\mathbf{t}_S(\mathbf{d}^{n,i}, \{[[\mathbf{u}]]\}^{n,i})\right\} \\ &\quad -\left[\mathbf{K}^S\right](\mathbf{d}^{n,i} - [\mathbf{P}]\{[[\mathbf{u}]]\}^{n,i}) = \mathbf{0}\end{aligned} \tag{60}$$

For a given $\mathbf{d}^{n,i}$, the system of non-linear equations (Eq. 60) can be solved for $\{[[\mathbf{u}]]\}^{n,i}$ and the element internal forces vector can be evaluated from Equation 59.

The rate form of Equations 59 and 60 can be cast into the following matrix form:

$$\begin{bmatrix}\mathbf{K}^{dd} & \mathbf{K}^{du} \\ \mathbf{K}^{ud} & \mathbf{K}^{uu}\end{bmatrix}\begin{Bmatrix}\dot{\mathbf{d}} \\ \{[[\dot{\mathbf{u}}]]\}\end{Bmatrix} = \begin{Bmatrix}\dot{\mathbf{f}}_{int} \\ \mathbf{0}\end{Bmatrix} \tag{61}$$

Condensing out $\{[[\dot{\mathbf{u}}]]\}$ yields:

$$\mathbf{K} = \mathbf{K}^{dd} - \mathbf{K}^{du}\left(\mathbf{K}^{uu}\right)^{-1}\mathbf{K}^{ud} \tag{62}$$

9 NUMERICAL TESTS

9.1 *Willam´s test*

To investigate the capacity of the proposed approach to represent multiple embedded discontinuities in the element, the test proposed by Willam et al. (1987) has been chosen.

The test is performed on a square plane stress element, whose geometry and boundary conditions are shown in Figure 5. The material parameters are: Young´s modulus, E=30 000 MPa; Poisson´s ratio, ν = 0.2; tensile strength, f_t= 3.0 MPaand fracture energy, G_F = 0.1 N/mm. The delta regularization parameter is assumed constant, k = 0.1 mm.

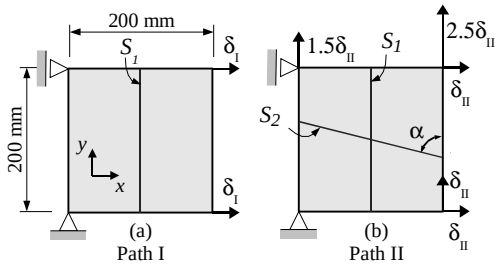

Figure 5. Willam's test: geometry and loads.

The initially uncracked specimen is subjected to two consecutive loading paths. In the first one, a monotonically increasing uniaxial tensile stress is applied in the x direction by increasing the horizontal displacement of the right nodes (see Fig. 5.a). The first loading path ceases when the stress reaches the tensile strength of the material and the first crack line, S_1, forms perpendicular to the first principal stress (see Fig. 5a).

The second loading path consists of a monotonically increasing of the nodal displacements according to the scheme shown in Figure 5.b. As a consequence, a strong rotation of the principal directions is imposed by increasing the in-plane total strains ε_{xx}, ε_{yy} and ε_{xy} in the proportion of 1.0: 1.5: 1.0.

A second crack is allowed to form at an angle perpendicular to the first principal stress if the stress state of the continuous portion of the element violates the initiation criterion again.

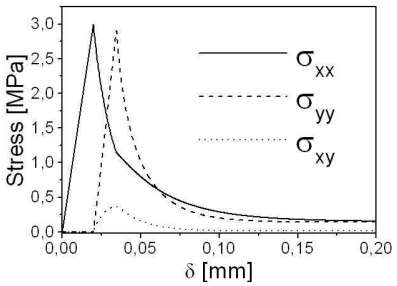

Figure 6. Willam's test: evolution of the stress components.

Figure 6 shows the evolution of the stress components σ_{xx}, σ_{yy} and σ_{xy}. In the second loading path, prior to the second crack initiation, the σ_{xx} stress component decreases while the other components increase due to the progressive rotation of the principal directions of strain. The softening behavior in crack S_1 causes a fast drop of the normal component σ_{xx} and it also prevents a significant increase of the shear component σ_{xy}.

Since the evolution of the normal component σ_{yy} is not affected by the crack, the stress state changes gradually from the initial simple tension in the *x* direction to a single tension in the *y* direction. When the stress state reaches the initiation criterion again, a second crack forms at an inclination angle of α=77.9° (see Figure 5.b). After the second crack initiation, all stress components decrease leading to a complete stress relaxation of the element.

9.2 *Three-point bending test*

To compare the performance of the approaches using uniform and non-uniform modes, the three-point notched beam tested by Peterson (1981) is chosen. The geometry, boundary conditions, and material parameters for this test are shown in Figure 7.

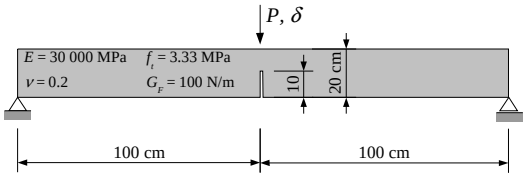

Figure 7. Three-point bending test.

The numerical analyses are performed using stress hybrid finite elements with uniform and non-uniform discontinuity modes. A single vertical crack is allowed to form in the element.

The Figure 8 shows the deformed meshes at a prescribed displacement δ = 0.2 cm. From this figure we observe that a crack line propagates upward from the notch tip, leading to a strong relative rotation between the two parts of the elements divided by the crack.

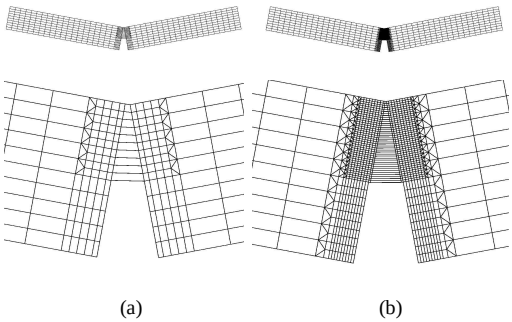

Figure 8. Deformed meshes: a) coarse mesh; b) fine mesh..

Since the finite element with uniform discontinuity modes are not able to accommodate a relative rigid-body rotation, the strains of the continuous portion are mobilized, preventing the stress relaxation of the element. The increasing load-displacement curves shown in Figure 9 reflects this stress-locking effect, even for a very fine mesh. Note in Figure 10 that the stress locking is completely removed by the consideration of non-uniform discontinuity modes and the resulting load-displacement curves obtained with the coarse and fine meshes are very close.

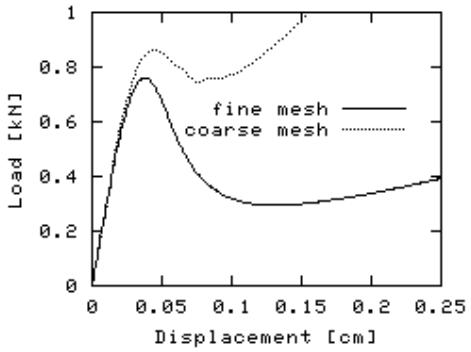

Figure 9. Load-displacement curve obtained with uniform discontinuity modes.

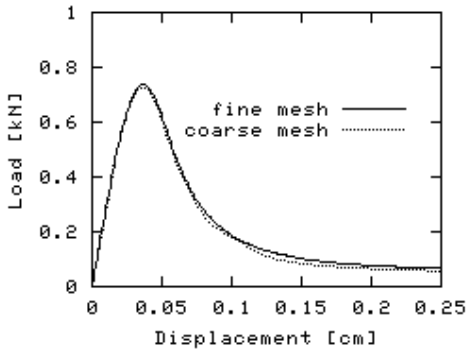

Figure 10. Load-displacement curve obtained with non-uniform discontinuity modes.

10 CONCLUSIONS

A technique to embed displacement discontinuities into stress hybrid elements has been presented. In this technique the element displacement field is split into two parts: a relative rigid-body motion due the displacement jump and the continuous displacement field of the solid part. The embedded discontinuity finite element formulation can then be obtained from the same variational functional used for the derivation of the underlying element (without discontinuity), but applied only to the

continuous portion of the element. The non-linear behavior in the discontinuity interface can be described by a discrete constitutive law or by a continuous one in the context of the strong discontinuity approach. The continuous portion and interface are coupled by enforcing traction continuity at collocations points of the interface.

As shown, this technique can be easily extended to represent multiple discontinuities interfaces as well as non-uniform discontinuity modes. The later formulation can be regarded as a particular case of the former.

The numerical studies show that the technique can be successfully applied to described internal discontinuity interfaces into stress hybrid elements.

The results of the three-point bending test show that the consideration of the non-uniform discontinuity modes is essential to avoid stress locking in cases involving a significant relative rotation between the parts of the element crossed by the discontinuity interface.

REFERENCES

Alfaiate, J. Wells G.N. & Sluys, L.J.. 2001. The use of embedded discontinuity elements with crack path continuity for mode-I and mixed-mode fracture, *Engineering Fracture Mechanics*,:69:661-686..

Dvorkin, E.N. Cuitino, A.M. & Gioia, G. 1990. Finite Elements with Displacement Interpolated Embedded Localization Lines Insensitive to Mesh Size and Distortions, *International Journal for Numerical Methods in Engineering*, 30: 541-564.

Jirásek, M. 2000. Comparative Study on Finite Elements with Embedded Discontinuities, *Comp. Methods Appl. Mech. Engineering*: 307-330.

Klisinski, M. Runesson, K. & Sture, S. 1991. Finite element with inner softening band, *ASCE, Journal of Engineering Mechanics*, (117) 3: 575-587.

Lotfi, H.R. & Shing, P.B. 1995. Embedded representation of fracture in concrete with mixed finite elements. *International Journal for Numerical Methods in Engineering*, 38: 1307-1325.

Manzoli, O.L. & Shing, P.B. 2002. Finite Elements with embedded multiple cracks and non-uniform discontinuity modes. In Benallal, A. & Proença, S.P.B. (ed.), *Recent Developments in the Modeling of Rupture in Solids*: 99-104. Paris.

Oliver, J. 1996a. Modeling Strong Discontinuities in Solid Mechanics via Strain Softening Constitutive Equations. part 1: Fundamentals, *International Journal for Numerical Methods in Engineering*, (39) 21: 3575-3600.

Oliver, J. 1996b. Modeling Strong Discontinuities in Solid Mechanics via Strain Softening Constitutive Equations. part 2: Numerical simulation, *International Journal for Numerical Methods in Engineering*, (39) 21: 3601-3623.

Oliver J. Cervera, M. & Manzoli, O.L. 1999. Strong Discontinuities and Continuum Plasticity Models: The Strong Discontinuity Approach, *Int. J. of Plasticity*, (15) 3: 319-351.

Pian T.H.H. 1995. State-of-the-art development of hybrid/mixed finite element method, Finite Elements in Analysis and Design, 21:5-20.

Simo, J.C. Oliver, J. & Armero, F. 1993. An analysis of strong discontinuities induced by strain-softening in rate-independent inelastic solids. *Computational Mechanics*, 12:277-296.

Simo, J.C. & Hughes, T.J.R. 1998. *Computational Inelasticity*, Springer-Verlag.

Spencer, B.W. & Shing, P.B. 2002. Stress hybrid embedded crack element for analysis of concrete fracture, In Willam, K. & Tanabe, T. (ed.), *Finite Element Analysis in Reinforced Concrete Structures*; *American Concrete Institute Special Publication*: SP 205.

Willam, K. Pramono, E. & Sture, S. 1987. Fundamental issues of smeared crack models, In Shah, S.P. & Swartz, S.E. (ed.), *Int. Conf. on Fracture of Concrete and Rock*:192-207, Society of Engng. Mech., Connecticut.

ACKNOWLEDGEMENTS

The financial support from the Brazilian Council for Scientific and Technological Development (CNPq) and the State of São Paulo Research Foundation (FAPESP) for this work is gratefully acknowledged by the first author.